Extended Manipulability Measure and Application for Robot Arm Equipped with Bi-articular Driving Mechanism

Kengo Yoshida[1], Naoki Hata[2], Sehoon Oh[1], Yoichi Hori[1]

[1]Department of Electrical Engineering
University of Tokyo
4-6-1 Komaba, Meguro
Tokyo153-8505, Japan
yoshida@horilab.iis.u-tokyo.ac.jp
sehoon@horilab.iis.u-tokyo.ac.jp

[2]Oki Electric Industry Co., Ltd.
3-16-11 Nishi Shimbashi, Minato-ku
Tokyo 105-8460, Japan
hata454@oki.com
hori@iis.u-tokyo.ac.jp

Abstract— **This paper describes an extended manipulability measure for robot arm based on bi-articular muscle principle. There are several manipulability measures for serial link manipulator. However they can not be applied for manipulators which has animal-like actuator alignment. Bi-articular muscle is an unique actuator of animals. It connects two joints and drives both simultaneously. Conventional measures does not consider such actuators. We extended Impedance Matching Ellipsoid (IME), which is an unified measure. Proposed measure considers animal-like actuator alignment including bi-articular muscles. For verification, we measured actual output force of robot arms. Whereas proposed measures can represent actual characteristics of the robot arm equipped with bi-articular driving mechanism.**

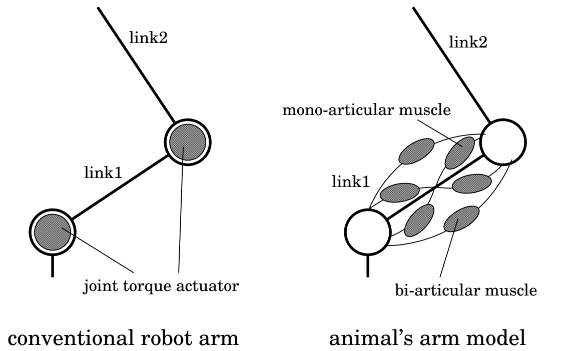

Fig. 1. Conventional robot arm model and animal's arm model

I. Introduction

In the 1980s and the early 1990s, several manipulability measures are proposed. Dynamic Manipulability Ellipsoid (DME) represents distributions of possible hand acceleration produced by normalized joint torque. Manipulating Force Ellipsoid (MFE) indicates transmission from normalized joint torque to distal force[1], [2]. Recently Kurazume et al. proposed Impedance Matching Ellipsoid (IME), which is an unified measure[3]. DME and MFE can be represented by special form of IME. IME characterizes dynamic torque-force transmission efficiency. These measures are used for analysis and design of robot arm.

However such conventional measures have a problem. They can not be applied for animal arm. Animal arm has complex alignment of muscles. Especially bi-articular muscle connects two joints and drives both simultaneously (Fig. 1). Conventional measures assume that each actuator drives respective joint independently, but bi-articular muscle does not. By existing bi-articular muscles, distal output characteristics are quite different compared to conventional robot arm. Our proposed extended measure considers above complex and redundant actuator alignments. Proposed measure can represent distal output characteristics of animal arm correctly. Proposed measure is verified by simulations and experiments.

Bi-articular muscle structure is ignored in traditional robotics. Recently important role of bi-articular muscle has emerged. Van Ingen Schenau et al. described that gastrocnemius muscle which is a bi-articular muscles in the calf of the leg develops and transmits propulsive force[4]. Mussa Ivaldi et al. reported changes of stiffness at end point of human arm[5]. Kumamoto et al. suggested modeling of human arms and legs using two antagonistic pairs of mono-articular muscles and one antagonistic pair of bi-articular muscles. They revealed that this model can explains recorded EMG patterns when human arms and legs output forces [6]. While several robots which mimic bi-articular muscle structure are proposed. Oshima et al. developed a jumping robot [7]. In their robot, knee and ankle joints are connected by wire. This wire mimics gastrocnemius muscle. They described gastrocnemius muscle controls a posture of their robot in vertical jump. Niiyama et al. proposed Mowgli, which mimics musculoskeletal system of frog[8]. Mowgli used pneumatic actuators and some of them drives two joints simultaneously. In our previous work, we proposed a robot design arm which has bi-articular driving mechanism[9][10].

In this paper, derivation of Extended IME is described in Section II. Verification by simulations and experiments are showed in Section III and IV respectively.

II. Derivation of Extended IME

A. Derivation of IME

This part briefly describes IME proposed by Kurazume et al. IME represents efficiency of torque-force transmission from joint torques to a load[3].

The dynamic equation of serial link manipulator is shown in Eq. (1). The manipulator has N links and N joints.

$$\boldsymbol{\tau} = \boldsymbol{M(q)\ddot{q}} + \boldsymbol{C(q,\dot{q})} + \boldsymbol{G(q)} + \boldsymbol{J(q)}^T \boldsymbol{F_e} \tag{1}$$

Here $\boldsymbol{\tau}$ is joint torques and $\boldsymbol{q}$ is joint angles. $\boldsymbol{M(q)}$ is a tensor of inertia. $\boldsymbol{C(q,\dot{q})}$ is Coriolis and centrifugal forces. $\boldsymbol{G(q)}$ is gravity force. $\boldsymbol{J(q)}$ is the Jacobian matrix. $\boldsymbol{F_e}$ is external force and moment applied to end point.

This manipulator hold a load at its end point. The dynamic equation of the load is shown in Eq. (2).

$$\boldsymbol{F_e} = \boldsymbol{M_p}(\boldsymbol{\ddot{x}} + \boldsymbol{\ddot{g}}) \tag{2}$$

Here $\boldsymbol{M_p}$ is mass of load. $\boldsymbol{\ddot{x}}$ is acceleration of load and it is equal to acceleration of end point of the manipulator. $\boldsymbol{\ddot{g}}$ is acceleration of gravity. Acceleration of end point is represented using the Jacobi matrix.

$$\boldsymbol{\ddot{x}} = \boldsymbol{J(q)\ddot{q}} + \boldsymbol{\dot{J}(q)\dot{q}} \tag{3}$$

From Eq. (1), (2) and (3), the dynamic equation of both the manipulator and the load is derived.

$$\begin{aligned}
\boldsymbol{\tau} &= \boldsymbol{Q(q)}(\boldsymbol{F_e} - \boldsymbol{F_{bias}}) \\
\boldsymbol{Q(q)} &= \boldsymbol{J(q)}^T + \boldsymbol{M(q)J(q)}^\dagger \boldsymbol{M_p}^{-1} \\
\boldsymbol{F_{bias}} &= (\boldsymbol{J(q)}^T + \boldsymbol{M(q)J(q)}^\dagger \boldsymbol{M_p}^{-1})^\dagger \\
&\times\ [\boldsymbol{M(q)J(q)}^\dagger(\boldsymbol{g} + \boldsymbol{\dot{J}(q)\ddot{q}}) - \boldsymbol{C(q,\dot{q})} - \boldsymbol{G(q)}]
\end{aligned} \tag{4}$$

F_{bias} is a bias term related to velocity and gravitation. Eq. (5) defines normalized torque $\boldsymbol{\tilde{\tau}}$.

$$\boldsymbol{\tilde{\tau}} = \boldsymbol{L}^{-1}\boldsymbol{\tau} \tag{5}$$

$\boldsymbol{L} = \mathrm{diag}(\tau_1^{\mathrm{limit}}, \tau_2^{\mathrm{limit}}, \ldots, \tau_{\mathrm{n}}^{\mathrm{limit}})$ represents maximum torque of each joint. Range of joint torque is represented by Eq. (6).

$$\boldsymbol{\tilde{\tau}}^T \boldsymbol{\tilde{\tau}} \le 1 \tag{6}$$

IME is derived from Eq. (4), (5) and (6).

$$(\boldsymbol{F_e} - \boldsymbol{F_{bias}})^T \boldsymbol{Q}^T (\boldsymbol{L^{-1}})^2 \boldsymbol{Q}(\boldsymbol{F_e} - \boldsymbol{F_{bias}}) \le 1 \tag{7}$$

MFE and DME are well-known measures. They are represented as limited forms of IME. When mass of load $\boldsymbol{M_p}$ is infinite, Eq. (7) is rewritten as Eq. (8). In this case IME is equal to MFE.

$$\boldsymbol{F}^T \boldsymbol{J(q)}(\boldsymbol{L^{-1}})^2 \boldsymbol{J(q)}^T \boldsymbol{F} \le 1 \tag{8}$$

When mass of load $\boldsymbol{M_p}$ is 0, Eq. (7) is rewritten as Eq. (9). In this case IME is equal to DME.

$$\boldsymbol{\ddot{X}}^T (\boldsymbol{M(p)J(q)}^\dagger)^T (\boldsymbol{L^{-1}})^2 (\boldsymbol{M(q)J(q)}^\dagger)\boldsymbol{\ddot{X}} \le 1 \tag{9}$$

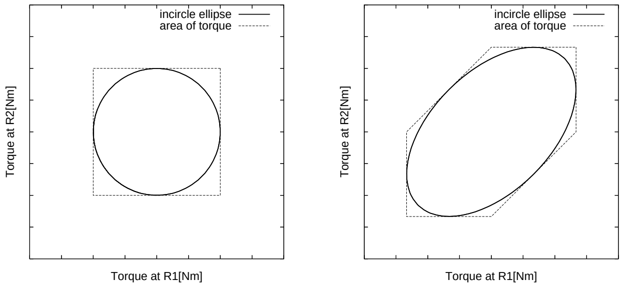

conventional robot arm　　animal arm

Fig. 2. Difference in Possible Range of Joint Torques Between Conventional Arm and Animal Arm

B. Considering Complex Actuator Alignment

Animal arm has complex actuator alignment. Above IME can not be applied to animal arm and robot arm which mimics animal muscular alignment. Fig. 2 shows difference in possible range of joint torque between conventional robot arm and animal arm. Each arm has two links and two joints but animal arm has bi-articular muscle which drives both two joints. In Fig. 2, outer polygonal shape indicates possible range of joint torque. Inner ellipse is inscribed to the polygonal shape and is representative of possible range. IME and other measures are mapping of this ellipse.

For considering complex actuator alignment, manipulator has N joints which is driven by M actuators. Some of actuators drive multiple joints simultaneously. A relation between joint torque $\boldsymbol{\tau}$ and torque of actuator $\boldsymbol{\tau_{act}}$ is Eq. (10).

$$\boldsymbol{\tau} = \boldsymbol{A_{lign}}\boldsymbol{\tau_{act}} \tag{10}$$

Where

$$\boldsymbol{A_{lign}} = \begin{pmatrix} a_{1,1} & a_{2,1} & \cdots & a_{M,1} \\ a_{1,2} & a_{2,2} & \cdots & a_{M,1} \\ \vdots & \vdots & \ddots & \vdots \\ a_{1,N} & a_{2,N} & \cdots & a_{M,N} \end{pmatrix} \tag{11}$$

Each element of actuator alignment matrix $\boldsymbol{A_{lign}}$ represents transfer coefficient form mth actuator to nth joint. $\boldsymbol{A_{lign}}$ is not regular matrix. Therefore pseudo inverse matrix is used for transfer from joint torque $\boldsymbol{\tau}$ to torque of actuator $\boldsymbol{\tau_{act}}$. Maximum torque of actuator is shown as $\boldsymbol{L_{act}} = \mathrm{diag}(\tau_1^{\mathrm{actlim}}, \tau_2^{\mathrm{actlim}}, \ldots, \tau_{\mathrm{m}}^{\mathrm{actlim}})$. Therefore normalized torque is represented by Eq. (12).

$$\boldsymbol{\tilde{\tau}_{act}} = c_{omp}\boldsymbol{L_{act}}^{-1}\boldsymbol{A}_{\boldsymbol{lign}}^{\dagger}\boldsymbol{\tau} \tag{12}$$

Here c_{omp} is compensation factor. Similarly extended IME is derived from Eq. (13) as Eq. (14)

$$\boldsymbol{\tilde{\tau}_{act}}^T \boldsymbol{\tilde{\tau}_{act}} \le 1 \tag{13}$$

$$(\boldsymbol{F_e} - \boldsymbol{F_{bias}})^T \boldsymbol{Q}^T \boldsymbol{E_{xtend}} \boldsymbol{Q}(\boldsymbol{F_e} - \boldsymbol{F_{bias}}) \le 1 \tag{14}$$

where

$$\boldsymbol{E_{xtend}} = c_{omp}^2 (\boldsymbol{L_{act}A_{lign}})^{\dagger T} (\boldsymbol{L_{act}A_{lign}})^{\dagger} \tag{15}$$

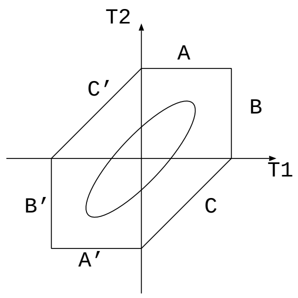

Fig. 3. Range of Joint Torques of 2 link manipulator

Extended MFE is rewritten as Eq. (16).

$$\boldsymbol{F}^T \boldsymbol{J(q)} \boldsymbol{E_{extend}} \boldsymbol{J(q)}^T \boldsymbol{F} \leq 1 \tag{16}$$

Extended DME is rewritten as Eq. (17).

$$\ddot{\boldsymbol{X}}^T (\boldsymbol{M(q)J(q)}^\dagger)^T \boldsymbol{E_{extend}} (\boldsymbol{M(q)J(q)}^\dagger) \ddot{\boldsymbol{X}} \leq 1 \tag{17}$$

C. Application for Two Link Manipulator with Bi-articular Muscles

Here we discuss about applying for two link manipulator with bi-articular. Fig. 3 shows possible range of joint torque in target manipulator. In this case $\boldsymbol{A_{lign}}$ and $\boldsymbol{L_{act}}$ is settled as Eq. (18) and (19).

$$\boldsymbol{A_{lign}} = \begin{pmatrix} 1 & 0 & 1 \\ 0 & 1 & 1 \end{pmatrix} \tag{18}$$

$$L_{act} = \mathrm{diag}(\tau_1^{\mathrm{actlim}}, \tau_2^{\mathrm{actlim}}, \tau_3^{\mathrm{actlim}}) \tag{19}$$

c_{omp} is adjusted so that IME touches hexagonal shape internally. $c_{ompA}, c_{ompB}, c_{ompC}$ are coefficients determined so that IME touches pair of edge A-A', B-B' and C-C' respectively. c_{omp} is chosen as Eq. (20).

$$c_{omp} = \max(\mathrm{c_{ompA}}, \mathrm{c_{ompB}}, \mathrm{c_{ompC}}) \tag{20}$$

Here $c_{ompA}, c_{ompB}, c_{ompC}$ are derived from condition to touch respective pair of edge.

$$c_{ompA} = \frac{1}{\tau_2^{actlim} + \tau_3^{actlim}} \sqrt{\frac{4e_{1,1}}{4e_{1,1}e_{2,2} - (e_{2,1} + e_{1,2})^2}} \tag{21}$$

$$c_{ompB} = \frac{1}{\tau_1^{actlim} + \tau_3^{actlim}} \sqrt{\frac{4e_{2,2}}{4e_{1,1}e_{2,2} - (e_{2,1} + e_{1,2})^2}} \tag{22}$$

$$c_{ompC} = \frac{4(e_{1,1} + e_{1,2} + e_{2,1} + e_{2,2})}{(\tau_1^{actlim} + \tau_2^{actlim})^2 \{4e_{1,1}e_{2,2} - (e_{1,2} + e_{2,1})^2\}} \tag{23}$$

$e_{1,1}, e_{1,2}, e_{2,1}, e_{2,2}$ are solved as the following.

$$(\boldsymbol{L_{act} A_{lign}})^{\dagger T} (\boldsymbol{L_{act} A_{lign}})^\dagger = \begin{pmatrix} e_{1,1} & e_{2,1} \\ e_{1,2} & e_{2,2} \end{pmatrix} \tag{24}$$

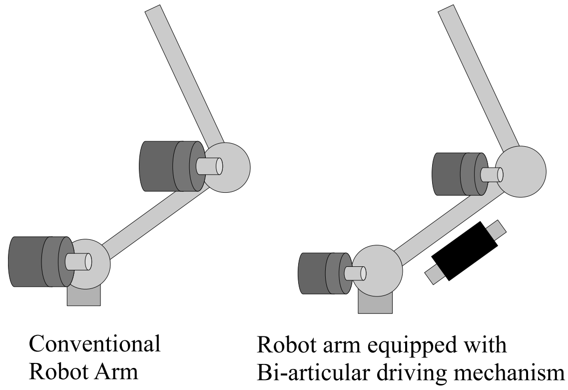

Fig. 4. Conventional Robot Arm and Target Robot Arm

D. Index of Manipulability

This part describes quantitative indexes of manipulability. These indexes are feature quantities of ellipsoid. Here singular values of $c_{omp}\boldsymbol{L_{act}}^{-1}\boldsymbol{A_{lign}}^\dagger\boldsymbol{Q}$ is defined as $\sigma_1, \sigma_2, ..., \sigma_N$ in descending order. Volume of ellipse is proportional to product of all singular values.

$$w_v = \sigma_1^{-1} \cdot \sigma_2^{-1} \cdot \ldots \cdot \sigma_N^{-1} \tag{25}$$

w_v is an index that indicates comprehensive efficiency of torque-force transfer.

w_m and w_r indicates balance of output.

$$w_m = \sigma_1^{-1} \tag{26}$$

$$w_r = \frac{\sigma_N}{\sigma_1} \tag{27}$$

w_m is corresponding to length of minor axis of ellipsoid and indicates minimum output at end point. w_r is equal to ratio between minor axis and major axis. w_r improves if ellipsoid is close to sphere.

III. Verification of Proposed Measure

This section describes verification of the proposed measure by simulation. Target model is two link manipulator, which works in horizontal plane. This manipulator has two joint, but these joints are driven by three actuators. Two actuators of them drives only one joint. One actuator drives two joints simultaneously. Fig. 4 shows target manipulator and conventional manipulator. For comparison, summation of maximum torque of actuators are same in both manipulators. Eq. (28) and Eq. (29) are maximum torque of actuators in target manipulator and conventional manipulator respectively.

$$\boldsymbol{L_{act1}} = \mathrm{diag}(\frac{2}{3}, \frac{2}{3}, \frac{2}{3}) \tag{28}$$

$$\boldsymbol{L_{act2}} = \mathrm{diag}(1, 1) \tag{29}$$

Each manipulator works in horizontal plane and each link is a thin rod. Parameters of the manipulators are shown in TABLE I. For verification of IME represented by Eq. (14),

TABLE I

Parameters of simulation model

l_1	length of link 1	1.0[m]
l_2	length of link 2	1.0[m]
m_1	mass of link 1	1.0[kg]
m_2	mass of link 2	0.5[kg]

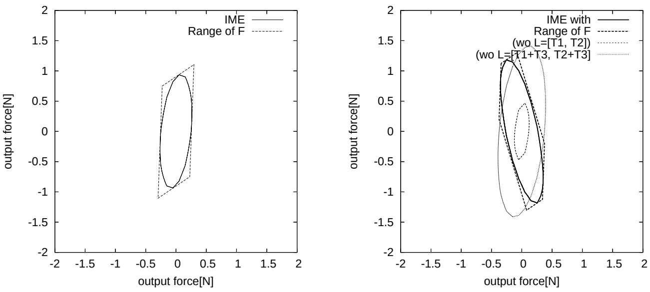

without bi-articular muscles   with bi-articular muscles

Fig. 5. IME and Range of Output Force Acting on the Load with or without Bi-articular Muscles

range of external force F_e applied to the load is solved by Eq. (30) directly.

$$\boldsymbol{F_e} = \boldsymbol{Q}^{\dagger}\boldsymbol{\tau} + \boldsymbol{F_{bias}} \tag{30}$$

Here mass of load is 0.5 kg and its velocity $\dot{\boldsymbol{x}}$ is 0. In this time, bias term $\boldsymbol{F_{bias}}$ becomes 0. Fig. 5 shows range of external force and IME ellipsoid about both manipulators.

Proposed measure can represent range of possible external force. In the right picture of Fig. 5, conventional measures are written as thin solid line. Small ellipse is result of ignoring bi-articular muscle. Assuming torque of bi-articular muscle drives both joint independently, conventional measure writes big ellipse. Each of them can not describe characteristics of actual range. Both volume and direction is incorrect in conventional measure.

IV. Experiment

A. Experimental Robot Arm

This part describes our experimental robot arm. This robot arm has two links and two joints. It works only in horizontal plane. Each joint is driven by the DC motor. Additionally this robot arm has a bi-articular driving mechanism consists of pulleys and belt. Bi-articular driving mechanism mimics animal bi-articular muscles. This mechanism drives both two joints simultaneously. Whole design of robot arm is shown in Fig. 6. Fig. 7 is photo of the robot arm. TABLE II shows major parts of the robot arm. TABLE III shows components of the control system. TABLE IV shows properties of the robot arm.

B. Experimental Verification

For experimental verification, the end point of the robot arm is fixed to the force sensor. Also the force sensor is fixed to the base of the machine (Fig. 8). The robot arm

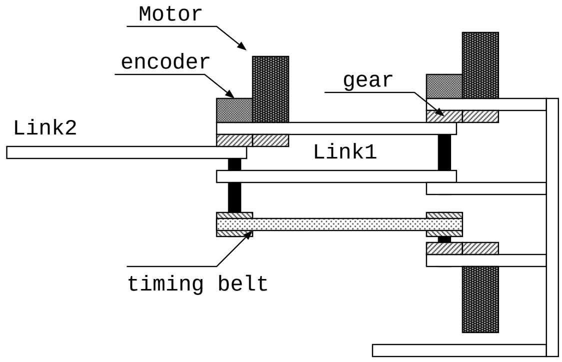

Fig. 6. Outline view of robot arm design

Fig. 7. A photo of robot arm

TABLE II

Major parameters of robot arm

Link1 (upper)	200×50×10[mm] 270[g]
Link1 (bottom)	200×50×10[mm] 270[g]
Link2	200×50×10[mm] 270[g]
Motors	TAMIYA(380K75)
Encoders	OMRON(E6H-CWZ6C)
Force Sensor	NITTA(IFS-67M25A25-l40-ANA)
Current Sensor	MAXON ADS 50/5

TABLE III

Components of control system

Motor driver	MAXON ADS 50/5
OS	ART-Linux
CPU	Intel Pentium4 1.5MHz
AD-DA board	Interface PCI-3523A
Counter board	Interface PCI-6201E
Receiver of force sensor	Nitta IFS-PCI-2184D

TABLE IV
PROPERTIES OF ROBOT ARM

Total height	270mm
Total length	500mm
Total mass of link 1	0.72kg
Total Length of link 1 between joint 1 and 2	165mm
Total mass of link 2	0.27kg
Total length of link 2 between joint 2 and center of force sensor	185mm
Moment of inertia of joint 1	0.034kg·m^2
Moment of inertia of joint 2	0.0058kg·m^2
Torque coefficient	0.20Nm/A

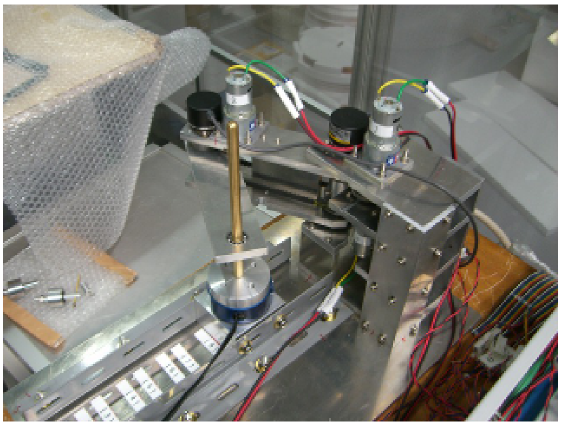

Fig. 8. Experimental Setup

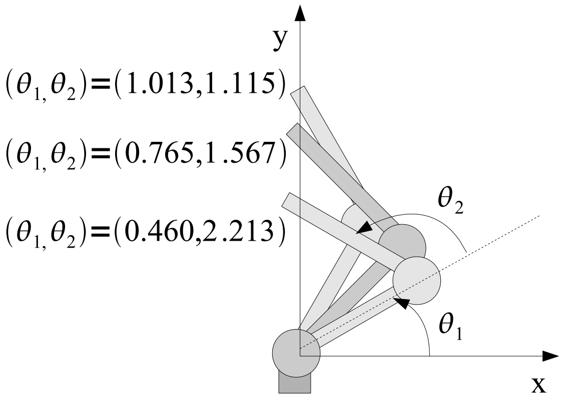

Fig. 9. Coordinate and Postures of Robot Arm

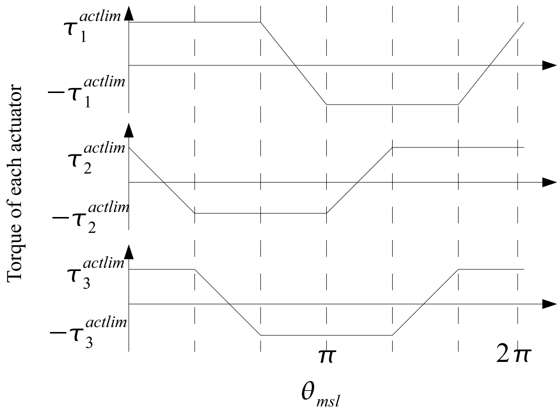

Fig. 10. Torque of actuators for robot arm equipped with bi-articular driving mechanism

generates maximum force for whole directions. The force sensor records output force at the end point of the robot arm.

In this experiment, mass of load $\boldsymbol{M_p}$ is regarded as ∞. IME is equal to MFE. Other parameters are based on TABLE IV. To generate maximum output force for each direction, torque of actuators are settled from Fig. 10 and 11. θ_{msl} is a variable only for convenience. We choose 40 torque set from $\theta_{msl} = 0$ to $\theta_{msl} = 2\pi$ evenly.

Fig. 12 shows result of experimental verification. Joint angles θ_1 and θ_2 are 0.765 rad and 1.567 rad respectively. In conventional arm (left picture), each motor generates maximum 0.3Nm. While in target arm (middle picture) each motor generates maximum 0.2Nm. Summation of maximum torque are same in each arm. Right picture shows the case that bi-articular driving mechanism is relatively big. Both joint motors generate 0.15Nm and bi-articular driving mechanism generates 0.3Nm. In these three pictures, polygonal shape is expected output force calculated by the Jacobi matrix. Actual recorded force is plotted as +. The ellipse drawn by dotted line indicates conventional or extended IME(MFE). Experimental result shows extended measure can represent characteristic of robot arm equipped with bi-articular driving mechanism. Characteristics of output force is significantly changed by output of bi-articular driving mechanism.

Fig. 13 and 14 are experimental results, when joint angles are changed. θ_1 and θ_2 are 1.013 rad and 1.115 rad in Fig. 13. The arm is in extended posture. θ_1 and θ_2 are 0.460 rad and 2.213 rad in Fig. 14. The arm is in flexed posture. These results show changes of characteristics by posture of the arm. Our proposed measure can represent these characteristics correctly.

V. CONCLUSION

This paper proposed extended manipulability measures and it can represent characteristic of the manipulator which has animal structure. Proposed measure is verified by the simulation and the experiment. In the experiment, our proposed bi-articular driving mechanism also works correctly.

Proposed measure can be applied to animal arms or robot arms which has animal characteristics. Proposed measure helps fair comparison of manipulability and effective design.

REFERENCES

[1] Tuneo Yoshikawa, "Dynamic Manipulability of Robot Manipulators", Journal of Robotic Systems, vol. 2, No. 1, pp. 113 - 124, 1985

[2] Stephen L. Chiu, "Task Compatibility of Manipulator Postures",

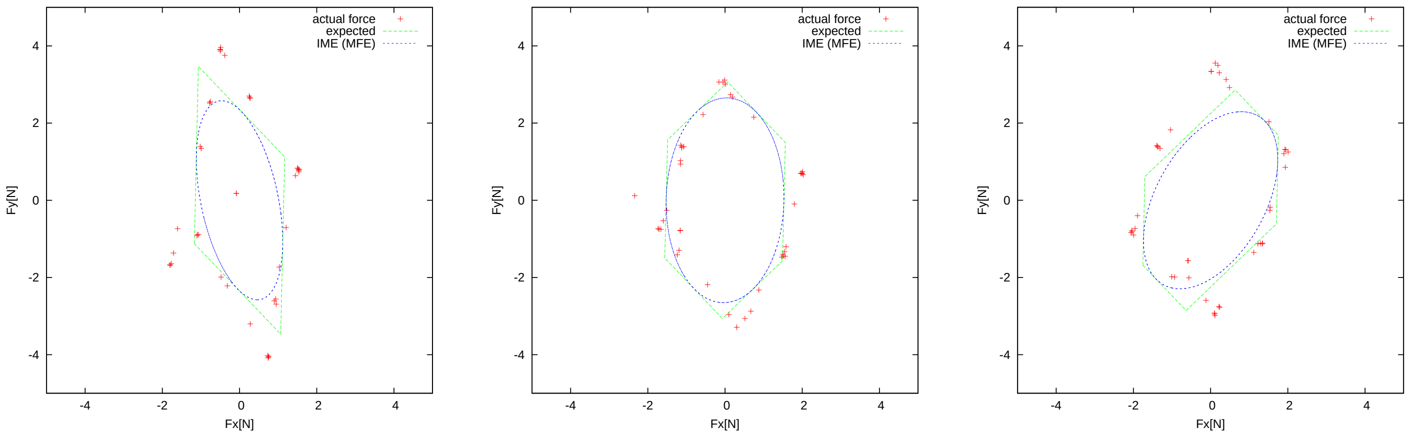

without bi-articular muscles
$\boldsymbol{L_{act}} = \mathrm{diag}(0.3, 0.3)$

with bi-articular muscles
$\boldsymbol{L_{act}} = \mathrm{diag}(0.2, 0.2, 0.2)$

with bi-articular muscles
$\boldsymbol{L_{act}} = \mathrm{diag}(0.15, 0.15, 0.3)$

Fig. 12. Experimental Result of Output Force of Robot Arm Equipped with Bi-articular Driving Mechanism

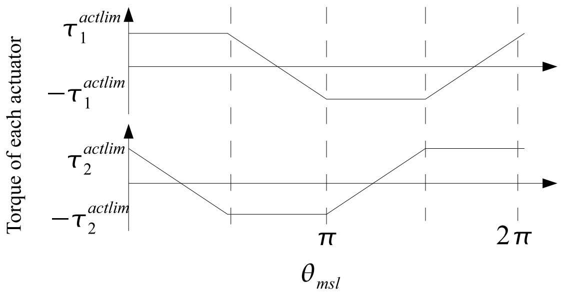

Fig. 11. Torque of actuators for conventional robot arm

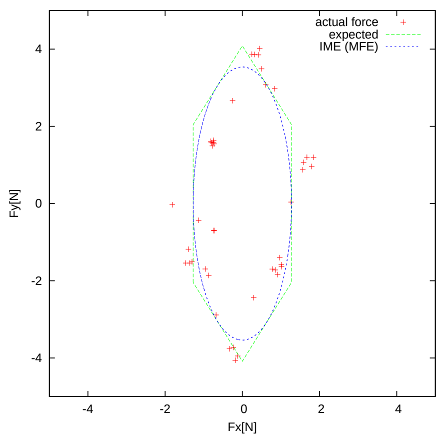

Fig. 13. Range of output force ($\theta_1 = 1.013, \theta_2 = 1.115$)

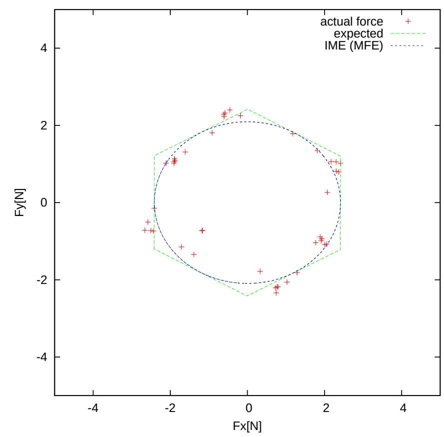

Fig. 14. Range of output force ($\theta_1 = 0.460, \theta_2 = 2.213$)

The International Journal of Robotics Research, vol. 7, No. 5, pp. 13 - 21, 1988

[3] Ryo Kurazume and Tutomu Hasegawa, “Impedance matching for a serial link manipulator”, Proceedings of the 2004 IEEE International Conference on Robotics & Automation, 2004

[4] G. J. van Ingen Shenau, M. F. Bobbert and R. H. Rozendal, “The unique action of bi-articular muscles in complex movements”, Journal of Anatomy, 155, pp. 1-5, 1987

[5] F. A. Mussa Ivaldi, N. Hogan and E. Bizzi, “Neural, Mechanical, and Geometric Factors Subserving Arm Posture in Humans”, The Journal of Neuroscience, Vol. 5, No. 10, pp. 2732-2743, 1985

[6] Mizuyori Kumamoto, Toru Oshima, Tomohisa Yamamoto, “Control properties induced by existence of antagonistic pairs of bi-articular muscles -Mechanical engineering model analyses”, Human Movement Science 13, pp. 611-634, 1994

[7] Toru Oshima, Noboru Momose and Kiyoshi Toriumi, “Jump mechanism using coordination in knee and ankle joint and application to leg orthosis” , The 2005 International Power Electronics Conference, 2005

[8] Ryuma Niiyama, Akihiko Nagakubo, Yasuo Kuniyoshi, “A bipedal jumping and landing robot with an artificial musculoskeletal system”, IEEE International Conference on Robotics and Automation, 2007

[9] Kengo Yoshida, Naoki Hata, Toshiyuki Uchida, Yoichi Hori, “A Novel Design and Realization of Robot Arm Based on the Principle of Bi-articular Muscles”, Proc. IEEE International Conference on Industrial Technology (ICIT), 2006. 12

[10] Kengo Yoshida, Toshiyuki Uchida, Yoichi Hori, “Novel FF Control Algorithm of Robot Arm Based on Bi-articular Muscle Principle - Emulation of Muscular Viscoelasticity for Disturbance Suppression and Path Tracking -”, IEEE IECON 2007, 2007